applied sciences

MDPI

Article

Generalising the Machine Tool Integrated Inverse Multilateration Method for the Ambient Thermal Error Analysis of Large Machine Tools in Industrial Environments

Fernando Egaña [1,*], Unai Mutilba [2], José A. Yagüe-Fabra [3], B. Ahmed Chekh [2] and Susana Lopez [1]

[1] Department of Mechanical Engineering, Tekniker, Basque Research and Technology Alliance (BRTA), C/Iñaki Goenaga 5, 20600 Eibar, Spain; susana.lopez@tekniker.es
[2] Department of Industrial Metrology, Tekniker, Basque Research and Technology Alliance (BRTA), C/Iñaki Goenaga 5, 20600 Eibar, Spain; unai.mutilba@tekniker.es (U.M.); brahim.ahmed@tekniker.es (B.A.C.)
[3] I3A, Universidad de Zaragoza, C/María de Luna 3, 50018 Zaragoza, Spain; jyague@unizar.es
* Correspondence: fernando.egana@tekniker.es; Tel.: +34-680655816

Featured Application: The machine tool integrated inverse multilateration (MIIM) methodology provides an effective solution for evaluating and compensating for thermal errors in medium- to large-sized machine tools operating in industrial environments with fluctuating ambient temperatures. The authors propose MIIM as a complementary tool to the current ISO 230-3 standard for determining thermal effects, offering a robust multi-point measurement approach. MIIM is particularly well-suited for factory acceptance testing, precision validation during machine installation, and long-term performance monitoring in non-thermally regulated workshops. Its adaptability to diverse machine architectures and numerical control systems underscores its potential for widespread application and enhancing machining accuracy and quality control in advanced manufacturing processes.

Abstract: This study expands on prior research by generalising the machine tool integrated inverse multilateration methodology to evaluate ambient thermal effects on medium- and large-sized machine tools in industrial environments. This method integrates an absolute distance measurement device into the machine tool spindle, enabling an automated and robust multilateration scheme without requiring controlled environments, expensive thermal instruments, or specialised artifacts. Tests were conducted using a LEICA AT960™ laser tracker and wide-angle retro-reflectors (both from Hexagon Manufacturing Intelligence, Stockholm, Sweden) across two machine architectures, THERA™ (gantry type) and ZERO™ (bed type), building on earlier work with the ARION G™ (bridge type), all of them MTs manufactured by Zayer (Vitoria, Spain). Sequential experiments in varying ambient conditions demonstrated the reliability of the machine tool integrated inverse multilateration approach over extended periods, showing strong correlations between the measured errors and temperature variations. The results were validated using a first-order mathematical model and finite element method simulations, confirming thermal error evolution as a function of ambient temperature changes. This method's adaptability to diverse machine architectures and industrial conditions highlights its potential for characterising and mitigating thermal errors in large machine tools. This work underscores the method's effectiveness and utility for advancing thermal error analysis in practical manufacturing settings.

Keywords: machine tool accuracy; thermal error analysis; MIIM methodology

Academic Editor: Wilma Polini

Received: 16 January 2025
Revised: 19 February 2025
Accepted: 26 February 2025
Published: 27 February 2025

Citation: Egaña, F.; Mutilba, U.; Yagüe-Fabra, J.A.; Chekh, B.A.; Lopez, S. Generalising the Machine Tool Integrated Inverse Multilateration Method for the Ambient Thermal Error Analysis of Large Machine Tools in Industrial Environments. *Appl. Sci.* **2025**, *15*, 2600. https://doi.org/10.3390/app15052600

1. Introduction

Thermal errors in machine tools (MTs) have been a subject of considerable research since their first identification by J. Bryan in the early 1960s [1]. These errors are widely acknowledged as a dominant factor that influences MT accuracy, accounting for between 60% and 75% of overall geometric deviations, as noted by Mayr et al. [2]. Due to their significant impact on precision manufacturing, investigations into thermal effects remain an active and evolving research domain [3], with numerous studies being published annually that explore innovative modelling, control, and compensation strategies.

Early studies, such as those by Ramesh et al. [4], introduced fundamental concepts in thermal error compensation, while Schwenke et al. [5] provided a classification framework distinguishing direct and indirect measurement methods for geometric errors. Subsequent work by Ibaraki et al. [6] concentrated on volumetric accuracy assessments using indirect techniques. More recent contributions, such as those by Li et al. [7] and Gao et al. [3], have expanded the field by addressing thermal error modelling and machine tool calibration. Additionally, the integration of machine learning into compensation methodologies, as demonstrated by Wang et al. [8], has introduced novel adaptive approaches for mitigating thermal effects in machining environments.

Thermal distortions that affect the tool centre point (TCP) can stem from two principal sources: internal heat generation within the machine structure and external environmental influences. Internal factors include thermal loads from motors, bearings, ballscrews, and frictional interactions during machining, which lead to localised temperature variations within the system. Conversely, external factors arise from ambient temperature fluctuations, and induce thermal expansion through convective heat transfer mechanisms. These external influences, often dictated by daily and seasonal cycles, have become increasingly significant as the manufacturing of larger components continues to demand tighter tolerances and higher precision [9]. The challenge of mitigating ambient thermal effects has been well documented in the literature [10–12], particularly given the high capital investment and operational costs associated with maintaining controlled workshop environments [13].

While historical research has predominantly focused on the thermal effects originating within machine components, there has been a recent shift towards analysing the impact of environmental thermal variations. For instance, Gross et al. [13] conducted extensive investigations in controlled conditions, placing an MT inside a climatic chamber to evaluate its response to stable ambient temperatures. More recent studies, such as those by Wei et al. [14,15], have examined seasonal temperature variations and their influence on MT spindles, proposing compensation models to mitigate these deviations. Similarly, Breitzke et al. [16] developed a long-term monitoring method for tracking thermal errors in three-axis machine tools using an INVAR-based artefact that was pre-characterised under stable conditions. Additionally, Brecher et al. [12] implemented a dynamic R-test, based on Weikert's methodology [17], to quantify five-axis machine tool deformations under fluctuating ambient conditions.

Advancements in digital twin technology have also contributed to the improved characterisation of thermal deviations. Iñigo et al. [18,19] developed a digital twin framework for predicting volumetric thermal distortions by leveraging rapid thermal characterisation techniques.

Beyond these methodologies, multilateration-based measurements employing tracking interferometers (TIs) have been explored as an alternative non-contact calibration method [20]. This approach estimates positional deviations by measuring distances between a retro-reflector at the TCP and fixed interferometers at the machine base. However, despite its precision, the lengthy data acquisition process limits the applicability of this approach in industrial settings, where the conditions are not fully controllable [3,13].

To overcome these challenges, rapid measurement techniques have been proposed. Ibaraki et al. [21] developed a spindle-heating test using a single interferometer within a two-dimensional plane, and this test was later refined by Mori et al. [22] to include additional displacement measurements for systems lacking rotary tables. Maruyama et al. [23] demonstrated that single-axis interferometry could effectively capture 2D positioning errors, mitigating thermal influences by reducing the measurement duration.

Additionally, Guillory et al. [24] introduced a cost-effective absolute multilateration system, replacing conventional TIs with a single ADM and four measuring heads, significantly lowering the implementation costs of simultaneous multilateration systems. Brosed et al. [25] further explored simultaneous laser multilateration using a telescopic instrument, eliminating the need for multiple TIs.

Among these methodologies, absolute interferometry has gained traction as a robust measurement approach. Schwenke et al. [26,27] pioneered the Multiline™ system, which employs multiple measurement lines anchored to key MT components to quantify thermal distortions.

Brecher et al. [28] later introduced an integrated laser-based technique that utilises a pentaprism, a laser source, and position sensitive devices (PSDs) to measure thermal-induced displacements within small and medium-sized MTs.

The ISO Standard 230-3:2020 [29] serves as the primary framework for evaluating environmental thermal influences on machine tools, enabling the characterisation of five degrees of freedom at a single measurement point. However, as noted by Mayr et al. [2], its applicability to medium and large MTs remains limited due to its restricted coverage of geometric error parameters. This underscores the necessity for alternative methodologies that are capable of minimising measurement uncertainty while addressing the complexities of temperature-induced distortions within an expanded working volume.

In light of these limitations, the present study extends previous research [30–33] by further developing a methodology to assess the ambient thermal effects on large machine tools within their operational workspace. The approach builds upon the machine tool integrated inverse multilateration (MIIM) method, which was initially introduced by Mutilba et al. [34]. While the initial results from single-machine experiments were promising, extending the methodology to other machine architectures is crucial for assessing its broader applicability. This study was conducted in two distinct industrial workshop environments, analysing two large-scale MTs under standard operational conditions without imposing artificial environmental constraints. Testing the methodology across varied working environments ensures its robustness, scalability, and general validity, revealing any architecture-dependent limitations. By incorporating an absolute distance measurement system into the MT spindle, the MIIM method enables a fully integrated multilateration-based assessment, mitigating the challenges associated with traditional techniques such as the use of climatic chambers, high-cost TIs, and artefact-based calibration, which are often impractical for large MTs.

Section 2 elaborates on the MIIM methodology, which employs a LEICA AT960™ (Hexagon, Stockholm, Sweden) laser tracker and four wide-angle retro-reflectors to facilitate automated, long-duration thermal assessments. This study evaluates two distinct MT architectures, the THERA™ (gantry type) and ZERO™ (bed type) architectures, expanding on prior investigations involving the ARION G™ (bridge type) architecture, all three of which are manufactured by Zayer MT builder (Vitoria, Spain).

Section 3 presents the experimental findings from sequential machine trials, first validating the method on the THERA™ system before extending it to the ZERO™ MT, which was tested under more demanding conditions. The recorded temperature variations exhibited a direct correlation with the thermal errors, which were analysed using both a first-order analytical model, following Zhang et al. [35], and a finite element method

(FEM) simulation [11,36]. These analyses confirmed that the observed error evolution was primarily driven by ambient temperature fluctuations.

Finally, Section 4 summarises the key findings, underscoring the potential of the MIIM approach for large-scale MT calibration in industrial environments. This study highlights its effectiveness in characterising environmental thermal errors, offering a scalable and automated solution for improving MT precision and stability in real-world machining applications.

2. Materials and Methods

An extensive series of tests have been conducted to demonstrate the broad applicability of the MIIM methodology for large machine tools, enabling the analysis of ambient temperature effects on variations in the machines' volumetric errors.

2.1. The Method—MIIM

This research is based on deploying the MIIM method developed by Mutilba et al. [34] in a fully automated manner to measure the machine tool's thermal drift across the entire volumetric workspace.

The proposed method integrates a tracking interferometer attached to the machine tool spindle, enabling an integrated multilateration measurement scheme as detailed in [30,33]. Thus, a predefined volumetric point grid is established for measurement, consisting of specific locations to which the machine tool directs the tracking interferometer for data acquisition. This sequential movement enables the interferometer to perform accurate distance measurements for four reflectors fixed to the machine tool table, which serve as reference benchmarks for the multilateration measurement scheme. These reflectors are strategically positioned on the machine tool table to ensure accurate and comprehensive spatial data acquisition.

As a result, the measurement approach operates continuously, reducing the measurement time to a single pass over the MT working volume and generating a volumetric error map of the machine every 40–50 min (depending on the size of the MT and the number of measurement points). This measurement frequency is sufficiently rapid to monitor and evaluate thermal errors induced by environmental temperature fluctuations over extended periods. Figure 1 illustrates the measurement setup for the Zayer ZERO™ machine tool under shop floor conditions. Thus, a LEICA AT960™ laser tracker is mounted on the tool holder using a specially designed support with a standard interface (HSK 100). For this specific test, four wide-angle retro-reflectors are positioned at the corners of the machine tool table.

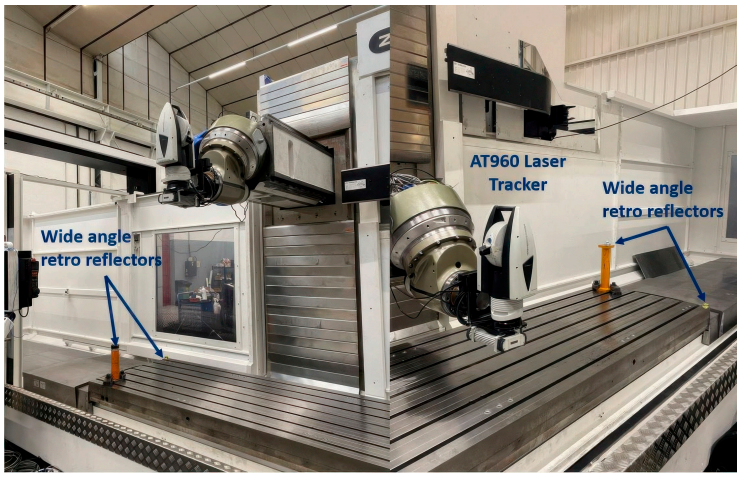

Figure 1. Wide-angle reflectors' disposition for the ZERO™ Zayer machine tool.

Table 1 summarises the key specifications of the laser tracker and retro-reflectors used during the MIIM tests. A LEICA AT960™ laser tracker was employed, which is based on an absolute distance meter (ADM) system [37].

Table 1. Laser tracker and retro-reflector characteristics.

	Manufacturer	Model	Range	Angle	U (k = 2)
Laser Tracker	Hexagon	AT960	20 m		10 µm + 0.4 µm/m
Retro-reflectors	Hexagon	Super Cat-Eye	18 m	±75°	*

* Data not available; implicit in the results.

The total number of points in the point cloud can be configured for each experiment, with the traversal path being customised to align with the specific objectives of the assessment. When the temperature fluctuates rapidly, a smaller number of points is selected to expedite measurements and minimise the overall duration of each measurement cycle. Conversely, when temperature changes are more gradual and a higher spatial resolution is required, a larger number of points is included in each sequence.

Figure 2 presents the spatial configuration of the point cloud along with the TCP positions, which are uniformly distributed across the XY, XZ, and YZ planes and strategically located within the mid-range of each axis. This arrangement of points is designed to enhance the efficiency of the inverse kinematics (IK) procedure, enabling the determination of MT kinematic parameters critical for potential volumetric adjustments. Starting from point P1, the machine sequentially progresses through each subsequent point until reaching the final point, thereby completing a full measurement cycle. Subsequently, the machine returns to point P1 to initiate a new measurement sequence.

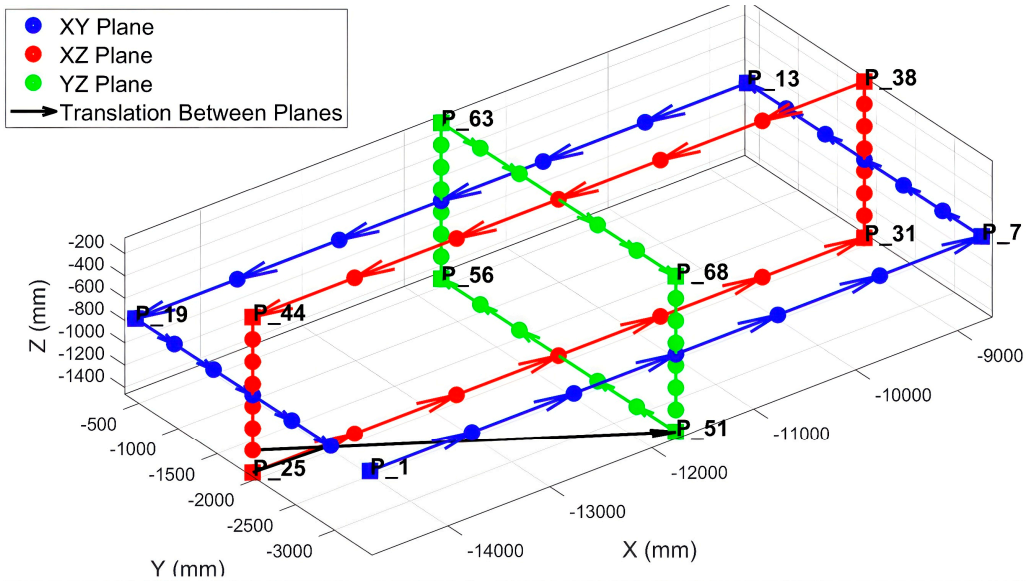

Figure 2. Measured points on the THERA™ Zayer MT.

For full automation of the measurement acquisition sequence, as explained in [30], it is essential to determine the spatial relationship between the reflectors positioned on the machine tool table and the laser tracker integrated into the machine tool spindle, and to do so all within the machine tool's coordinate system. This relationship is established by performing two sequential best-fit transformations at four corner points within the machine tool's working volume.

The first best-fit transformation aligns the laser tracker reference system with the reflectors fixed on the machine tool table. This is accomplished by sequentially moving the

machine tool to four corner points of the point grid, where the laser tracker, embedded in the machine's spindle, measures the 3D positions of fiducial points at each corner. This transformation aligns the four data sets, establishing the spatial relationship between the corner points of the point cloud and the fiducial points within a local coordinate system established at the initial measurement station.

The second best-fit transformation transfers this data set to the machine tool coordinate system. This is achieved by transforming the coordinates of the four corner points to fit the MT coordinate system using their nominal coordinates.

The full automation of the MIIM measurement process eliminates the need for human intervention throughout the entire duration of the batch measurement sequence. This ensures that, as soon as a volumetric error mapping process is completed, the system seamlessly initiates a new measurement sequence. Consequently, hundreds of volumetric error mapping measurements can be conducted fully autonomously over several consecutive days. This process is enabled through closed-loop communication between the laser tracker controller and the machine tool controller. As the machine tool moves to the next measurement point within the point cloud, the laser tracker controller receives a trigger to perform distance measurements at each fiducial point. Similarly, once the laser tracker completes its measurement, the machine tool controller is signalled to proceed to the next measurement point.

The closed-loop communication between the laser tracker controller and the machine tool controller is orchestrated by the metrology software that is used to execute the measurement sequence. Thus, the SpatialAnalyzer® 2023.2 software (Hexagon, Stockholm, Sweden) is utilized, providing all the necessary functionalities to facilitate seamless bidirectional communication with the machine tool controller.

As illustrated in Figure 3, the laptop running the metrology software is connected to the laser tracker controller (integrated into the machine tool head) and the machine tool controller via the machine's PLC using a TCP/IP connection. Alternatively, for long tests, the laser tracker can also connect wirelessly via a Wi-Fi network.

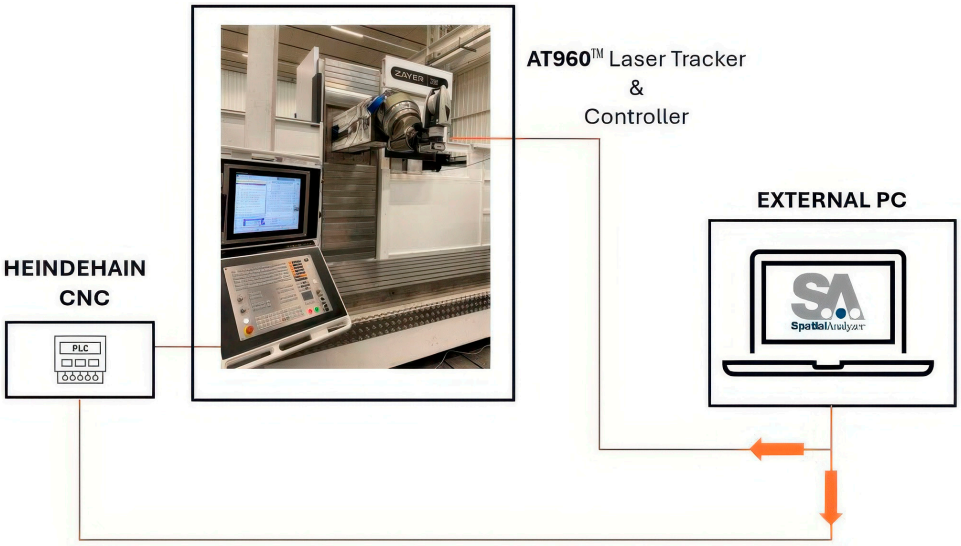

Figure 3. Connection setup between the laser tracker and machine tool controllers.

On the laser tracker controller side, signal transmission and reception are managed using various functionalities provided within the Measurement Plan environment of Spatial Analyzer®. On the machine tool controller side, specific logic has been implemented within the machine tool's PLC environment to enable signal exchange. This is achieved through a

CNC logic-based subprogram, which facilitates the modification of CNC variables within the machine's PLC.

In this setup, the main measurement CNC program, introduced by the technician, invokes the subprogram to enable CNC variable modifications, allowing the measurement process to operate in a fully autonomous mode.

Currently, this capability has been established for HEIDENHAIN TNC7 (Dr. Johannes Heidenhain GmbH, Traunreut, Germany) and SIEMENS 840 C (Siemens AG, Munich, Germany) controllers.

2.2. Research Materials—Tested Machine Tools

This research was conducted on two Zayer machine tools, each characterised by distinct architectural designs. The research builds upon the analyses previously performed on the ARION G™, which was used for the preliminary research documented in [30,33]. The current study examines the THERA™ machine, where the solution was extended to the Heidenhain CNC, and the ZERO™ machine, where all final validations were also conducted using the same CNC. Figure 4 depicts the two machines under study, with the THERA™ on the left and the ZERO™ on the right.

Figure 4. Zayer machine tools examined in this research: (**a**) THERA™ machine, and (**b**) ZERO™ machine.

Table 2 summarises the main characteristics of the machine tools used in this research, which focused on developing and validating the MIIM methodology for measuring the impact of ambient thermal effects on machine tools.

Table 2. Main characteristics of the tested machine tools.

	ARION G™	**THERA™**	**ZERO™**
Architecture	Bridge	Gantry	Bed
Linear Axes	X part side Y, Z Tool side	X, Y, Z Tool side	X part side Y, Z Tool side
Travel X (mm)	3500	14,500	4000
Travel Y (mm)	3100	3500	1200
Travel Z (mm)	1100	1500	1600
Shop floor	Tekniker	Zayer	Zayer
Climatization	No	Yes 20 °C ± 1 °C	Heating ≤ 20 °C

This experimental research was complemented by simulation studies employing the FEM to analyse the theoretically expected thermal response of each machine under investigation. Figure 5 presents the FEM models of both machines, with the ram positioned

at the ends of their respective travel ranges. Both models consider the anchorages to the floor as fixed points in the boundary conditions.

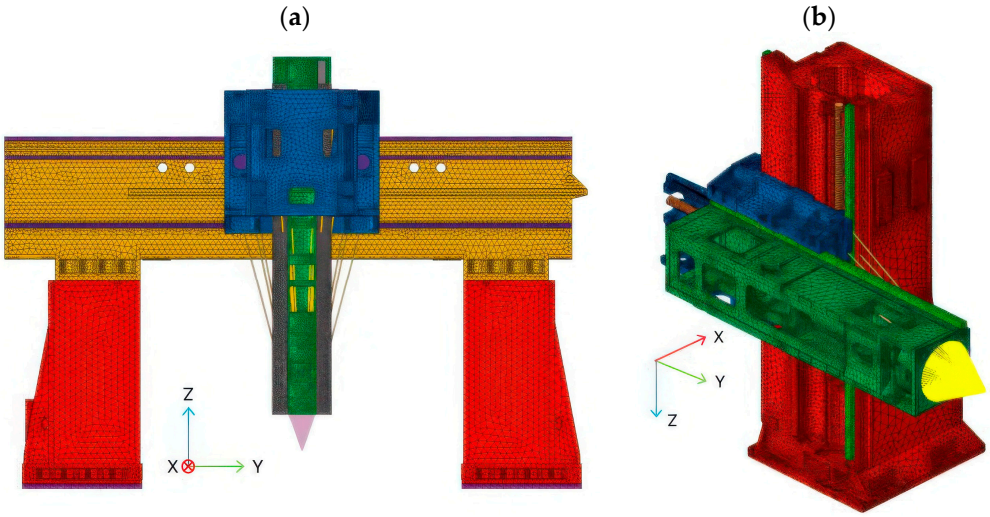

Figure 5. Machine tool FEMs: (**a**) THERA™ machine and (**b**) ZERO™ machine.

Table 3 outlines the key specifications of the ambient temperature sensor used to monitor the air temperature near the ram of the tested machine. No additional thermal sensors were incorporated into the experiments to minimise supplementary measurement equipment and in order to rely solely on the laser tracker system.

Table 3. Ambient temperature sensor main characteristics.

Sensor Type	Measuring Range	Accuracy	Resolution	Reaction Time	Calibration
Pt-100	−100 to +260 °C	±(0.3 °C + 0.3% of mv)	0.01 °C	<45 s	ISO/IEC-17025

In the THERA™ machine tool, due to its symmetrical design, the most sensitive direction to thermal errors caused by ambient temperature variation is the Z-direction (vertical), corresponding to the contraction and elongation of the columns and ram. In the case of the ZERO™ machine tool, with the thermo-symmetric design of its column, the ram's contraction and elongation again represent the most sensitive component, generating errors primarily in the Y-direction.

Figure 6 depicts the thermal deformation in the critical direction for the tested machines during a stationary step of −1 °C, showing a significant contraction in the Z direction on the THERA™ MT and in the Y direction on the ZERO™ MT.

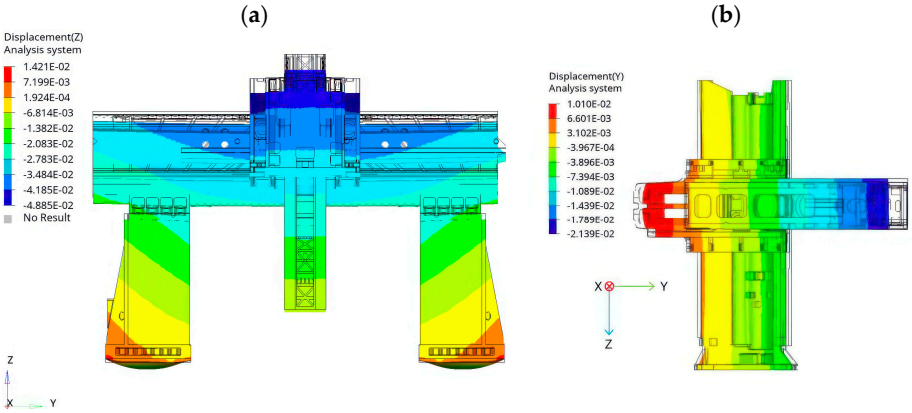

Figure 6. Stationary thermal deformation (mm) under ΔT = −1 °C. (**a**) THERA™ and (**b**) ZERO™.

3. Experimental Tests and Results

The following research was conducted to validate the MIIM methodology for evaluating errors by large-scale MTs caused by variations in the ambient temperature and to generalise its application to other MT architectures beyond those employed in previous studies. Prior to this work, all experiments had been restricted to a single machine within a single environment. In contrast, this research involves extensive testing on two different machines in two distinct environments, providing a broader scope for analysis.

3.1. THERA™ Machine Tests

From 23 October to 7 November 2023, a series of tests were conducted on the THERA™ Zayer gantry machine at the Zayer assembly shop floor. The objective was to validate the robustness of extending the MIIM methodology—previously applied to a single machine with a SIEMENS 840 CNC—to a new MT architecture equipped with a HEIDENHAIN TNC7 CNC control.

Several experiments were conducted over two weeks, defining a measurement point cloud of 74 points, with each MIIM measurement requiring 48 min to complete. Figure 7 illustrates the linear axis reference system used and provides a detailed view of the laser tracker mounted on the tool holder during the measurement procedures. The measured volume and resolution for each measurement were as follows:

- X-axis: −14,700 ÷ −8700 (6000 mm) with a step size of 1000 mm; portal frame gantry movement;
- Y-axis: −3400 ÷ −400 (3000 mm) with a step size of 500 mm; transverse movement along the bridge;
- Z-axis: −1460 ÷ −60 (1400 mm) with a step size of 200 mm; ram vertical movement.

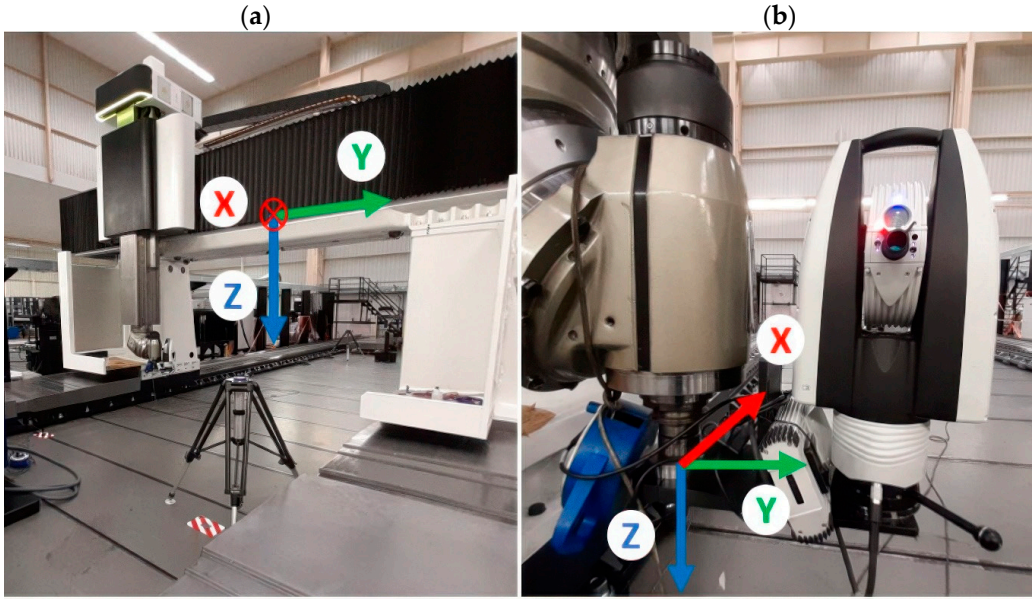

Figure 7. THERA™ machine tool axes definition: (**a**) general view of the machine tool and (**b**) laser tracker on the tool holder.

Refer to Figure 2 for a detailed representation of the point cloud utilised in the test campaign conducted on the THERA™ machine tool. The figure illustrates the spatial distribution of points and the sequence of movements for each MIIM measurement.

The machine was placed in a large environment dedicated to the assembly, setup, and factory acceptance testing of MTs before they are dispatched to the final user. The shop floor was thermally controlled during working hours, maintaining the air temperature at

20 °C ± 1 °C. The temperature control system was switched off at 6:00 p.m. and reactivated at 5:00 a.m. daily.

Figure 8 depicts the air temperature variations during the test campaign, illustrating how the temperature was effectively maintained during working hours on weekdays, decreased overnight, and recovered quickly when the climate control system was reactivated before the start of daily operations. Two tests are reported: the first was conducted over three weekdays with minimal temperature variations, and the second was conducted over eight days, including a weekend. The image highlights the weekends and 1st November, when the air-conditioning system was also turned off, resulting in the lowest recorded temperatures, particularly during the second weekend, when the ambient temperature dropped to a minimum of 16.87 °C.

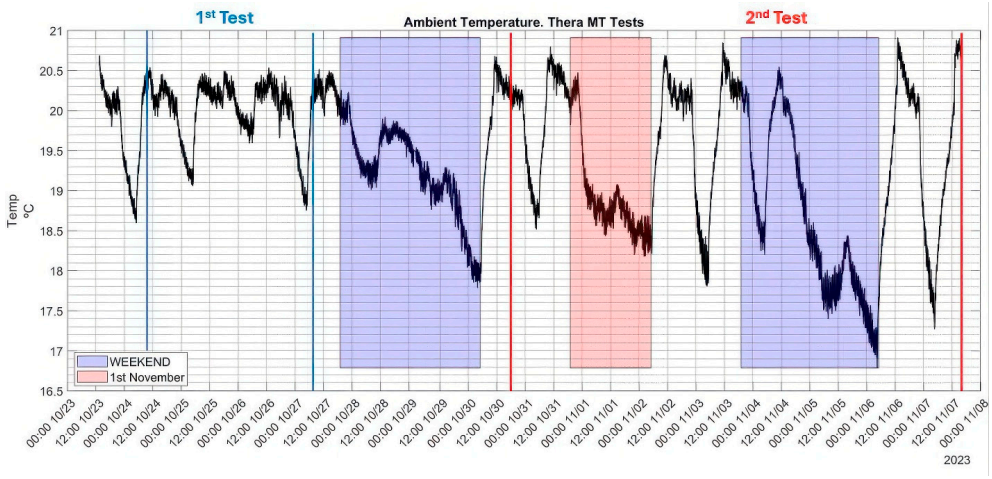

Figure 8. Measured air temperature near the THERA^{TM} machine.

Table 4 summarises the ambient temperature variations, across which there was an an average temperature close to 20 °C due to the controlled environment. A maximum difference of 4 °C was recorded during the second experiment, which was attributable to the three non-working days included in the test.

Table 4. Average, maximum, minimum, and absolute ambient temperature variations recorded on tests conducted during October–November 2023 on climatised shopfloor.

Test Days	Taverage (°C)	Tmax (°C)	Tmin (°C)	ΔT (°C)
24–27 October	19.99	20.50	18.79	1.71
30 October–7 November	19.21	20.85	16.87	4.02

3.1.1. First Test: Low Ambient Temperature Variation

The first test was conducted over three consecutive working days without interruptions and under stable ambient temperature conditions. This near quasi-stationary scenario was achieved due to the climate-controlled shop floor, which maintained stable temperatures during the day. Additionally, warm nights resulted in minimal overnight temperature drops, with variations of less than 1 °C. During this period, 86 complete MIIM measurements were performed.

Figure 9 shows the geometric deviations at each of the 74 measured points (refer to Figure 2) across the 86 MIIM measurements conducted from 24 to 27 October 2023. The average ambient temperature during this period was approximately 20 °C, fluctuating between a minimum of 18.8 °C and a maximum of 20.5 °C (refer to Table 4), with very stable conditions during working hours. The superimposed data in the figure, forming a narrow

band, highlight the minimal repeatability error of the MIIM methodology compared to the absolute geometric error of the MT. Geometric deviations along the X, Y, and Z axes are denoted as Ex, Ey, and Ez, respectively.

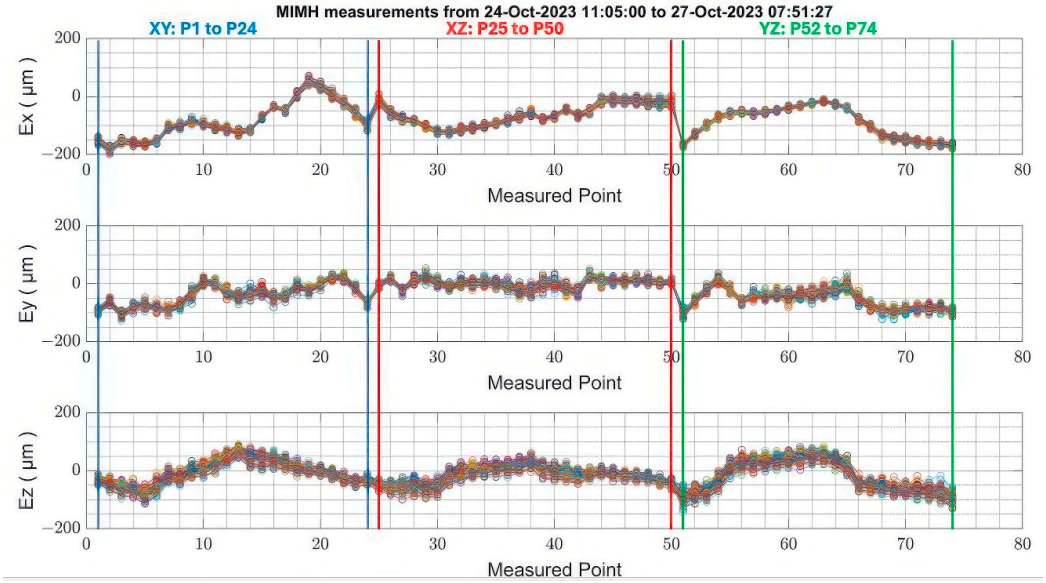

Figure 9. Measured geometric deviation for THERA^{TM} MT axes Ex, Ey, and Ez (first test: low ambient temperature variation).

Table 5 provides the maximum and average standard deviation values for the X, Y, and Z axes that were calculated for this experiment, referring to Figure 9.

Table 5. Maximum and average standard deviation values for the MIIM test performed from 24 to 27 October 2023 (results in µm).

	X-Axis (µm)	Y-Axis (µm)	Z-Axis (µm)
Average	5	8	12
Maximum	10	12	17

The results indicate that the volumetric errors or deviation variations were small during this experiment. However, even under stable ambient conditions, the machine tool errors exhibited a delayed response to the temperature trends. Due to the symmetrical design of the machine, this effect was most prominent along the Z-axis, where the columns and ram expanded or contracted in proportion to ambient temperature changes (refer to Figure 6).

Figure 10 illustrates the evolution of the environmental temperature variation error (ETVE) in the Z direction at a specific point within the measurement point cloud, corresponding to a Y-centred position and maximum ram extension (Point P_25 in Figure 2). A clear correlation is observed between temporal fluctuations in the point deviation and ambient temperature changes. As the temperature increases, the error grows in a positive direction, effectively making the machine appear larger, with a certain delay. Conversely, as the temperature decreases, the error shifts in a negative direction, making the machine appear smaller. The error remains stable in the absence of temperature fluctuations.

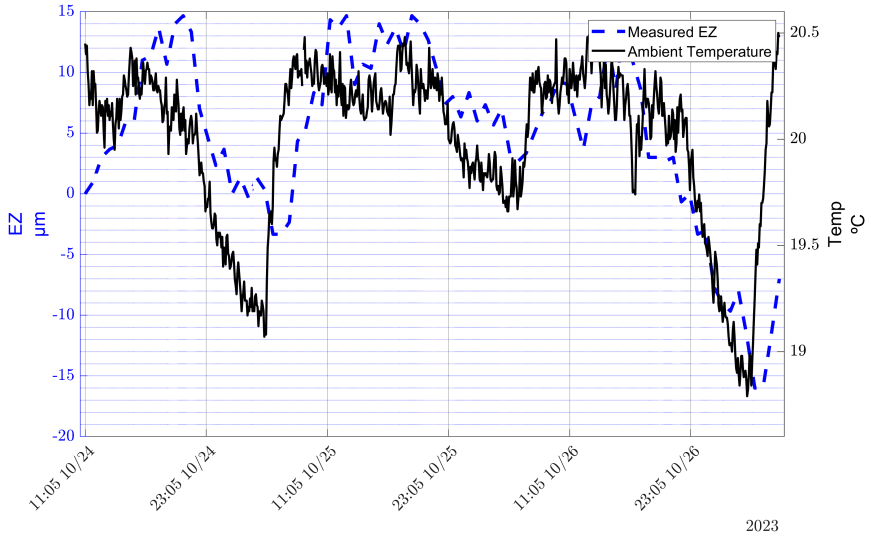

Figure 10. Air temperature and ETVE in Z direction from 24 October to 27 October.

3.1.2. Second Test: Extended Duration and Greater Environment Variability

The second significant test was conducted over eight uninterrupted days, during which the ambient temperature exhibited greater variations compared to the first test. While the shop floor's climate control system maintained a stable temperature during working hours, colder nights, particularly on 1 November and during the weekend climate control shutdown, resulted in a significant temperature drop of 4.0 °C. Over this period, a total of 225 complete MIIM measurements were performed. The average ambient temperature during the eight-day experiment was 19.21 °C, with temperatures ranging from a minimum of 16.8 °C to a maximum of 20.9 °C. Highly stable conditions were observed during working hours due to the climatization system.

Figure 11 illustrates the deviations at each of the 74 measured points (refer to Figure 2) across the 225 MIIM measurements conducted between October and November 2023. Geometric deviations along the X, Y, and Z axes are represented as Ex, Ey, and Ez, respectively.

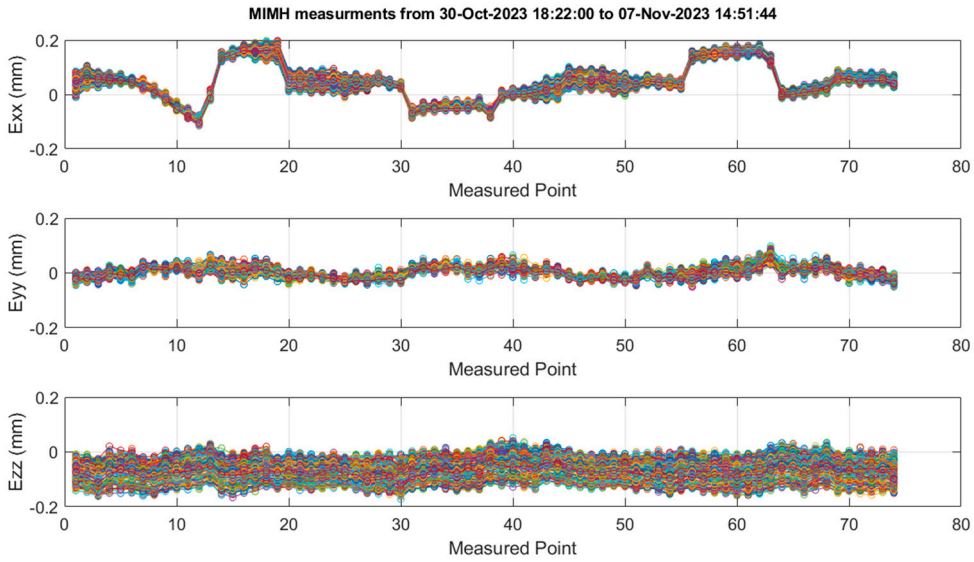

Figure 11. Measured points' geometric deviation per THERA^{TM} MT along axes Ex, Ey, and Ez under varying environmental conditions.

Table 6 presents the average and maximum standard deviation values for the X, Y, and Z axes, calculated based on the data shown in Figure 11.

Table 6. Maximum and average standard deviation values for the MIIM test performed between 30 October and 7 November 2023 (results in μm).

	X-Axis (μm)	Y-Axis (μm)	Z-Axis (μm)
Average	12	8	33
Maximum	21	15	37

Figure 12 shows the evolution of the ETVE in the Z direction at a specific point within the measurement point cloud, corresponding to a Y-centred position and maximum ram extension (Point P_25 in Figure 2). A clear correlation is evident between temporal fluctuations in the point deviation and the ambient temperature changes. As the temperature increases, the error grows in a positive direction, effectively making the machine appear larger, with a certain delay. Conversely, when the temperature decreases, the error shifts in a negative direction, making the machine appear smaller. The error remains stable in the absence of temperature fluctuations.

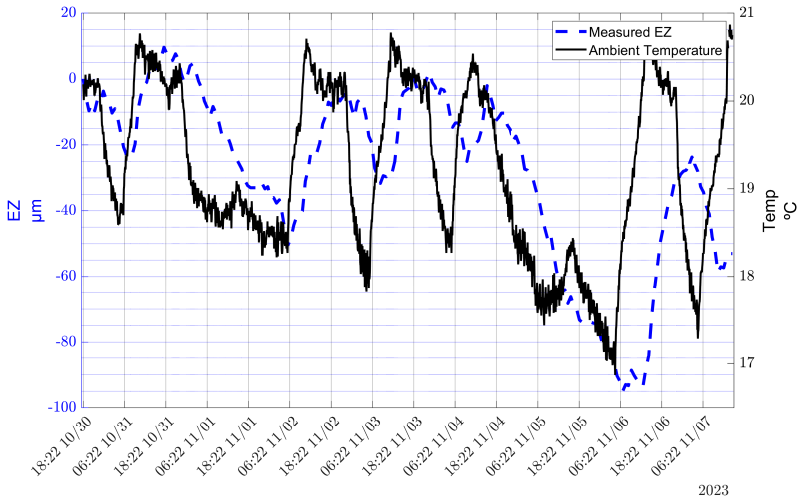

Figure 12. Air temperature and ETVE in Z direction from 30 October to 7 November.

3.2. ZERO™ Machine Tests

Between 12 and 26 February 2024, a new test campaign was conducted on the ZERO™ Zayer machine on the Zayer manufacturing shop floor. This campaign aimed to extend the MIIM methodology to a Heidenhain TNC7 CNC control system and assess its applicability to a different MT architecture, specifically a bed-type machine located in a non-climatised environment. Unlike previous tests, this environment had only a heating system for operator comfort, resulting in significant temperature variations during the two-week experiment.

Several experiments were conducted during this period, defining a measurement point cloud comprising 84 points. Each MIIM measurement required 46 min and 24 s to complete. Figure 13 shows the linear axis reference system and details of the laser tracker mounted on the tool holder during the measurement procedures. The measured volume and resolution for each measurement were as follows:

- X: ÷ 2.650 ÷ −1.350 (1.300 mm) with a step size of 260 mm (table horizontal movement);
- Y: −1.300 ÷ −100 (1.200 mm) with a step size of 240 mm (ram horizontal movement);
- Z: −1.150 ÷ −50 (1.100 mm) with a step size of 100 mm (vertical movement along the column).

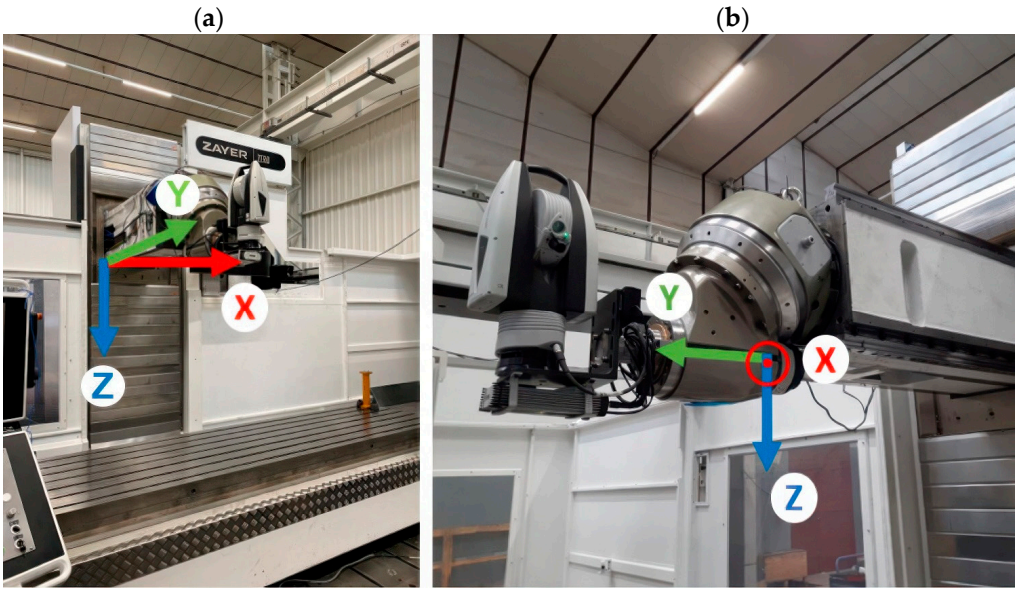

Figure 13. ZERO™ machine test details: (**a**) reference system and (**b**) detail of the laser tracker attached to the tool holder.

Figure 14 illustrates the point cloud and movement sequence used in this test campaign, conducted on the ZERO™ machine tool.

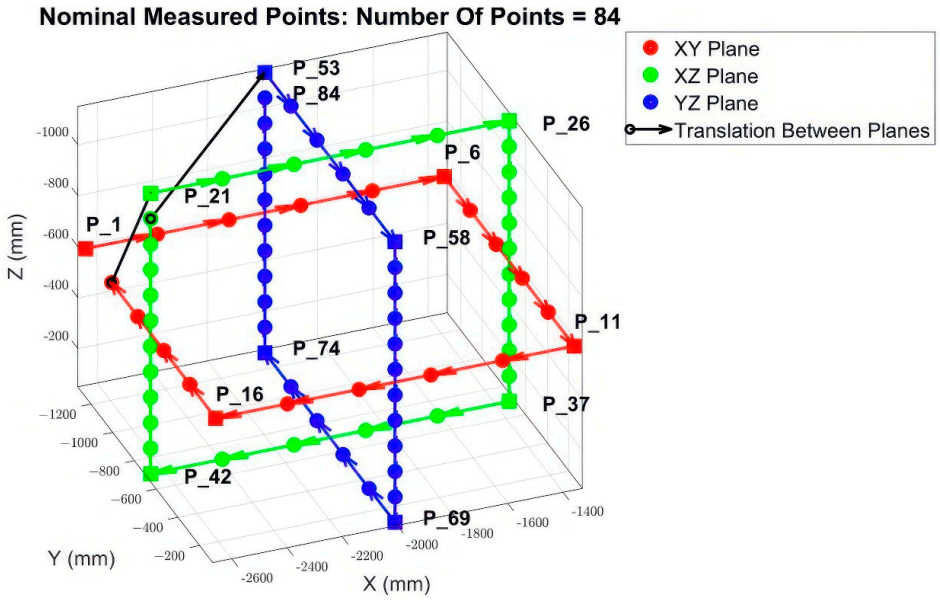

Figure 14. Measured points' spatial distribution and movement sequence for the ZERO™.

Two significant experiments, each lasting over three days and involving more than 100 complete MIIM measurements, are detailed in the following sections. These experiments confirm the methodology's value in studying thermal errors induced by ambient temperature variations within a machine tool's working volume. The first experiment was conducted over three working days with substantial temperature fluctuations, while the second, longer experiment spanned a similar duration but included a weekend.

Figure 15 depicts the evolution of the air temperature during the test campaign, showing significant drops during the night, with reductions of nearly 8 °C on the coldest nights. Rapid temperature recovery occurred each morning when the heating system was activated a few hours before the start of the workday. The test campaign also included two weekends.

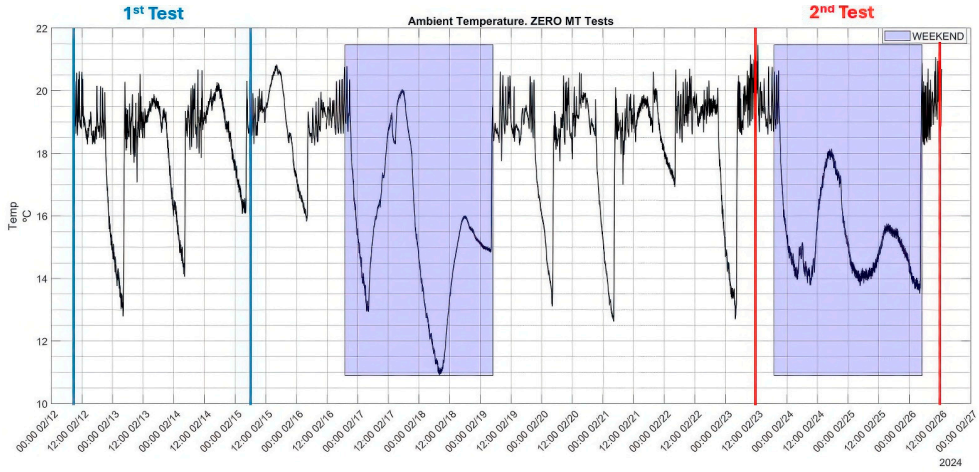

Figure 15. Measured air temperature near the ZERO^{TM} machine.

Table 7 summarises the notable ambient temperature variations, with differences of nearly 8 °C being observed due to the heating system being switched off during the night and over weekends.

Table 7. Average, maximum, minimum, and absolute ambient temperature variation recorded by a test conducted in February 2024 in a non-climatised shopfloor.

Test Days	Taverage (°C)	Tmax (°C)	Tmin (°C)	ΔT (°C)
12–15 February	18.25	20.58	12.86	7.72
23–26 February	16.18	21.37	13.56	7.81

The results for the three axial directions indicate a strong correlation between the temperature variations and error evolution. The errors consistently shifted in the same direction as the temperature changes, with a slight delay and smoother transitions due to the thermal inertia of the machine's structure.

Figures 16–18 illustrate the temperature evolution and corresponding measured error evolution for each axis during the two selected tests. These results pertain to Point P_11, representing the maximum ram extension and an intermediate position along the Z direction.

Refer to Figures 13 and 14 for additional context. In all figures, the absolute value of the error increases in in a negative direction, indicating that the machine appears to contract as the ambient temperature drops during the night. The error tends to recover during the rapid morning temperature increase when the shop floor heating system is reactivated.

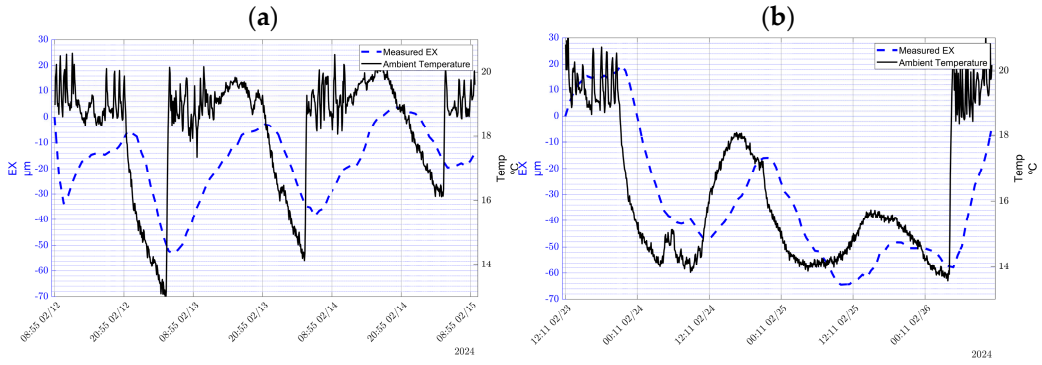

Figure 16. Temporal evolution of error E_X: (**a**) first test from 12 to 15 February and (**b**) second test from 23 to 25 February.

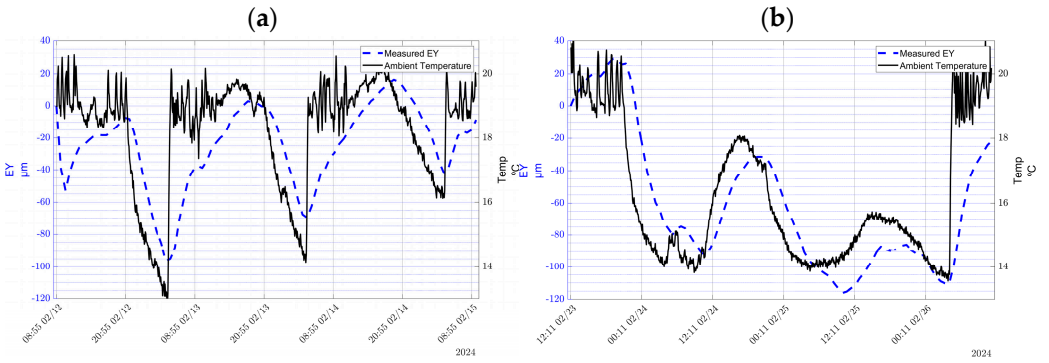

Figure 17. Temporal evolution of error E_Y: (**a**) first test from 12 to 15 February and (**b**) second test from 23 to 25 February.

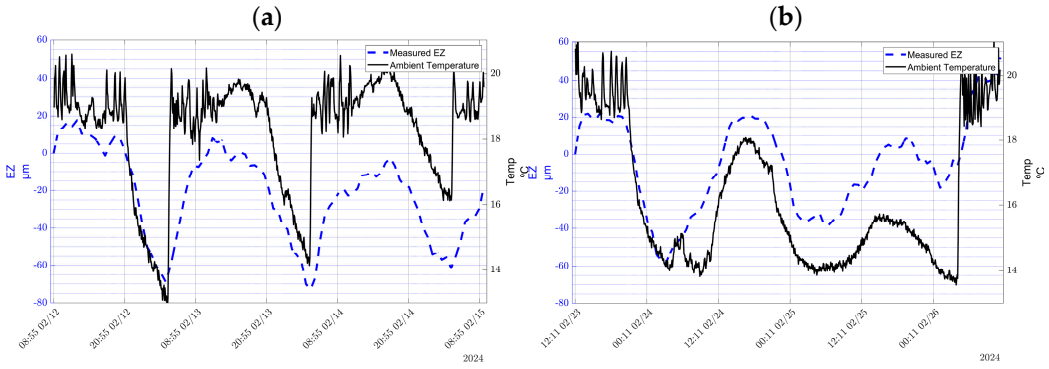

Figure 18. Temporal evolution of error E_Z: (**a**) first test from 12 to 15 February and (**b**) second test from 23 to 25 February.

Two theoretical approaches were undertaken to mathematically validate that the measured error evolution depicted in the above figures was caused by ambient temperature variations:

- First-Order Model: A first-order model was calibrated using data from one of the tests to identify key parameters, including the thermal time constant and proportional gain. This model was then used to generate a simulated response based on the temperature data from the first test. A comparison of the simulated output with the actual measured errors demonstrated a strong correlation, confirming the model's accuracy.
- Finite Element Method Analysis: The second approach entailed utilising the machine's FEM model to perform a transient thermal analysis, using temperature variations as the input. The predicted deformations were compared with the measured errors, once again validating that the observed error evolution is attributable to ambient temperature fluctuations.

3.2.1. First-Order Model Validation of ZERO™ Machine Tests

To explain the measured error values, an initial attempt was made to derive the thermal error transfer function by fitting a simple physical model to the results. This model utilised the ambient temperature as the input and the evolution of the measured error as the output. A similar methodology was recently proposed by Zhang et al. [35]. The hypotheses for establishing the model are as follows:

- The energy balance in each direction is modelled as a single thermal inertia. The heat loss or gain of the machine is assumed to be proportional to the temperature difference between the machine and its environment, with radiative effects being considered negligible;

- The heat transfer coefficient is treated as a constant, independent of the temperature and direction, whether heat is transferred from the machine to the environment or vice versa;
- The machine's expansion is assumed to be essentially linear concerning the temperature;
- All variables are considered to deviate from the baseline operating conditions, under which the errors were initially defined as zero.

By modelling the energy balance in each direction as a single thermal inertia, the calculation is conducted based on the formula presented in Equation (1).

$$m \times C_p \times \frac{dT}{dt} = U \times A \times (T_{env} - T) \tag{1}$$

wherein the following definitions apply:

- m: the considered mass of the structure;
- C_p: specific heat capacity of the structural material;
- U: the convective heat transfer coefficient;
- A: the effective convective area;
- T_{env}: the environment temperature difference;
- T: the temperature difference of the structure.

The length variation with the temperature can be expressed as follows

$$\alpha \times L_{initial} \times \frac{dT}{dt} = \frac{dL}{dt} \tag{2}$$

wherein the following definitions apply

- α: the linear expansion coefficient of the structural material;
- $L_{initial}$: specific initial length at the instant where the conditions were set to zero.

Applying the Laplace transformation to the above Equations (1) and (2), Equations (3) and (4) are obtained.

$$m \times C_p \times s \times T(s) = U \times A \times (T_{env}(s) - T(s)) \tag{3}$$

$$\alpha \times L_{initial} \times T(s) = L(s) \tag{4}$$

Combining Equations (1) and (2) and rearranging them, the following transfer function between the position error and the ambient temperature is obtained:

$$m \times \frac{L(s)}{T_{ext}(s)} = \frac{\alpha \times L_{initial} \times U \times A}{U \times A + m \times C_p \times s} = \frac{\alpha \times L_{initial}}{1 + \frac{m \times C_p}{U \times A} s} \tag{5}$$

wherein:

- System gain: $k = \alpha L_{initial}$;
- Time constant: $\tau = \frac{m \times C_p}{U \times A}$.

To identify the system, the tfest function from the MATLAB™ R2022a System Identification Toolbox (Mathworks, Natick, MA, USA) was utilised to analyse a three-day data set collected from 23 to 26 February. Data from the second test were selected for the model calibration, as they were gathered during a weekend, thus avoiding interference from other machinery and providing an environment that was likely to exhibit larger temperature differences.

The measurements used to adjust the model were taken at three distinct positions along the Y-axis of the ram. The sampling frequency for the training data was 46 min and

24 s, which corresponds to the time required to complete one full MIIM cycle. The model's input was the difference between the ambient temperature and the initial temperature, while the output represented the measurement error in the Y-axis position relative to the initial measurement

Table 8 presents the results of the identification process, including the system gains and time constants derived from the experimental data recorded at three different selected points. Further details can be found in Figure 14.

Table 8. Identified system parameters.

Position	Maximum Ram Extension	Middle Ram Extension	Minimum Ram Extension
Measured Point			
Travel Y (mm)	−100	−700	−1300
k (mm/°K)	0.02	0.014	0.011
τ (s)	13,773	14,653	15,079

The thermal time constants at the three Y-measured positions are found to be quite similar. When $U \times A$ is calculated for all cases, values ranging from 48 to 53 W/K are obtained. Assuming a specific heat capacity C_p of 460 J/kg·K, as specified in EN 1561:2024 for grey cast iron [38], a ram mass (m) of 1580 kg, and an effective surface area of the ram in contact with the environment of approximately 5 m^2 (A), the convection coefficient (U) is estimated to be around 10 W/m^2·K. This appears to be a reasonable value for natural convection at moderate temperatures

Once the model was developed, an initial analysis was conducted by comparing the model's output with the measured data to assess its performance.

Figure 19 presents the training data used to identify the model parameters as expressed in Equation (5). This includes the measured E_Y error evolution at Point P_11 alongside the simulated values representing the output of the adjusted first-order model at the same point. This point corresponds to the maximum extension of the ram.

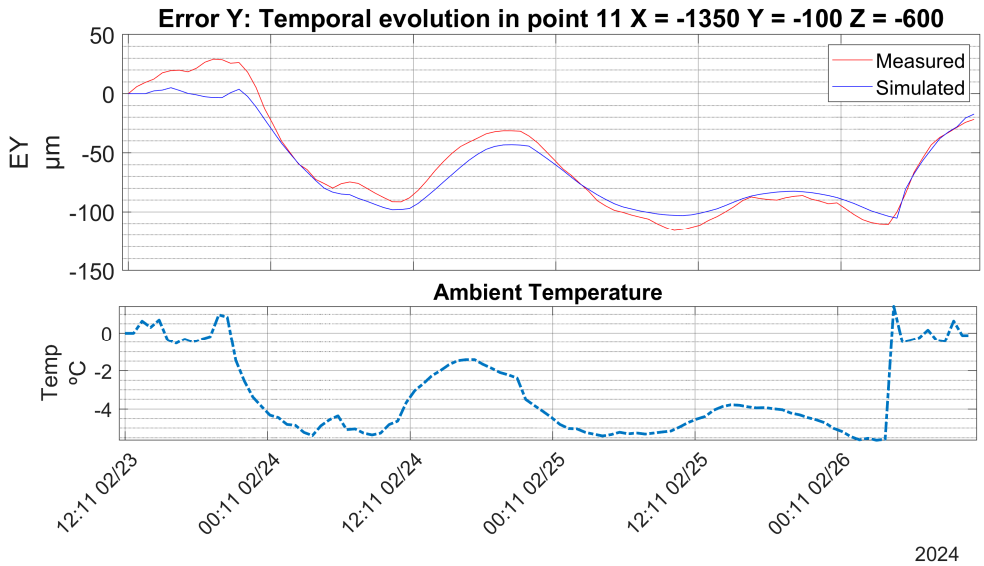

Figure 19. Training data to identify the first-order model parameters and the corresponding model results. From 23 to 26 February.

Figure 20 presents a second analysis conducted to validate the first-order model. This involved comparing the model's output, generated using ambient temperature data from the initial test period from 12 to 15 February as the input, against the MIIM output recorded during the same period.

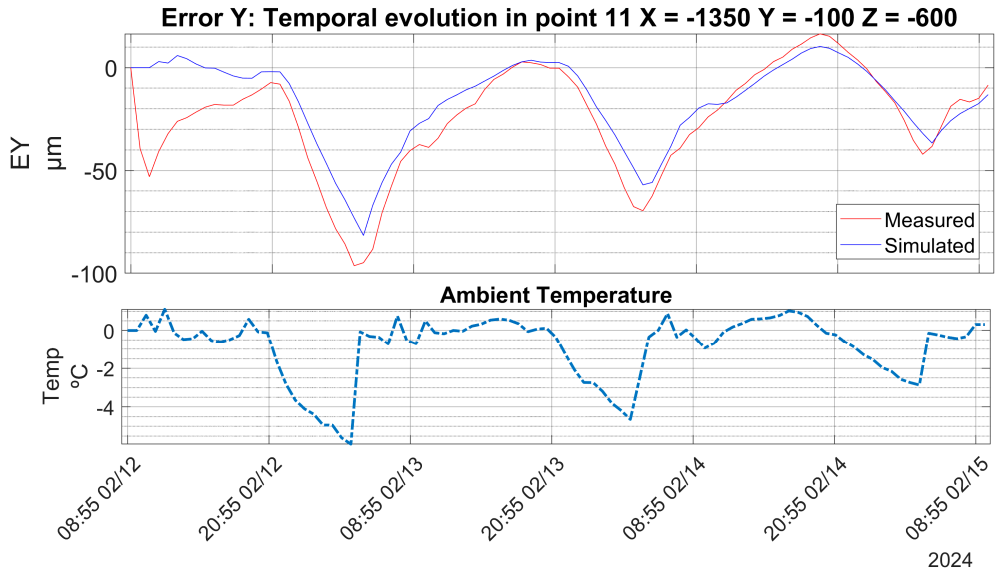

Figure 20. Validation of the first-order model output against real measured data from the initial test. From 12 to 15 February.

Several metrics were employed to evaluate the quality of the model, demonstrating that the output, namely the machine error variation, is directly related to the model's input, which is the recorded ambient temperature. The following metrics were used:

$$MAE = \frac{1}{N} \times \sum_{i=1}^{N} |y_i - \hat{y}_i| \tag{6}$$

$$RMSE = \sqrt{\sum_{i=1}^{N} \frac{(y_i - \hat{y}_i)^2}{N}} \tag{7}$$

herein, the following definitions apply:

- y_i: Measured value at time instant i. In this case, it represents the ETVE in the Y direction obtained from the MIIM measurement;
- $\hat{y}_i$: Estimated or predicted value at time instant i. This is the estimated E_{TVE} in the Y direction, as calculated by the adjusted first-order model;
- N: Number of data points; in this case, 100 MIIM results;
- Mean absolute error (*MAE*): Calculated as the sum of the absolute differences between the predicted values (calculated by the model) and the actual measured values divided by the sample size;
- Root mean square error (*RMSE*): The quadratic mean of the differences between the measured values and the predicted values.

Table 9 presents the numerical values of the established metrics, comparing the measured data with the predictions generated by the first-order model for the two analyses. The comparison between the model's output and the measured data revealed a strong correlation, demonstrating that the model accurately predicts the machine's error variation, which is primarily influenced by the ambient temperature. The model's performance was quantitatively assessed using the MAE and RMSE metrics, which confirmed the model's validity in both the adjustment phase (22–26 February) and the subsequent validation phase (12–15 February). The lower MAE and RMSE values during the adjustment phase (6.9 µm and 9.6 µm, respectively) compared to the validation phase (10.1 µm and 14.1 µm) indicate that the model performs well within the calibration range, although there is some discrepancy when it is applied to a different period.

Table 9. Comparison metrics between measured values and first order model predictions.

	Date	MAE [µm]	RMSE [µm]
Adjustment	22 to 26 February	6.9	9.6
Validation	12 to 15 February	10.1	14.1

3.2.2. FEM-Based Validation of ZERO™ Machine Tests

A second approach was undertaken to validate the correlation between the measured thermal error evolution and environmental temperature variations using FEM simulations. The ZERO™ machine was modelled using Altair Optistruct™ 2024 Software (Altair Engineering Inc., Troy, MI, USA), as shown in Figure 5b. A transient thermal analysis was conducted using the recorded environmental temperature variations from 23 to 26 February as input data. The analysis output, representing the TCP displacement at each of the 100 calculated steps, was then compared with the errors measured at the corresponding steps during the MIIM process.

Several points within the point cloud were analysed to confirm the validity of the simulation results, which yielded good correlations across all tested positions. For clarity, the results for two significant and easily interpretable positions are presented below, where they are compared in detail with the experimentally measured errors from the MIIM tests.

Figure 21 shows the calculated positions corresponding to Point P_11 and Point P_31 (refer to Figure 14). These positions are critical for determining the Y-axis error and are particularly sensitive to environmental temperature variations, as previously explained. Position 1 is expected to exhibit a greater degree of influence from temperature changes, with a proportional relationship to the intermediate position. This behaviour aligns with a convective heat transfer scenario and the linear expansion characteristics of the structural material.

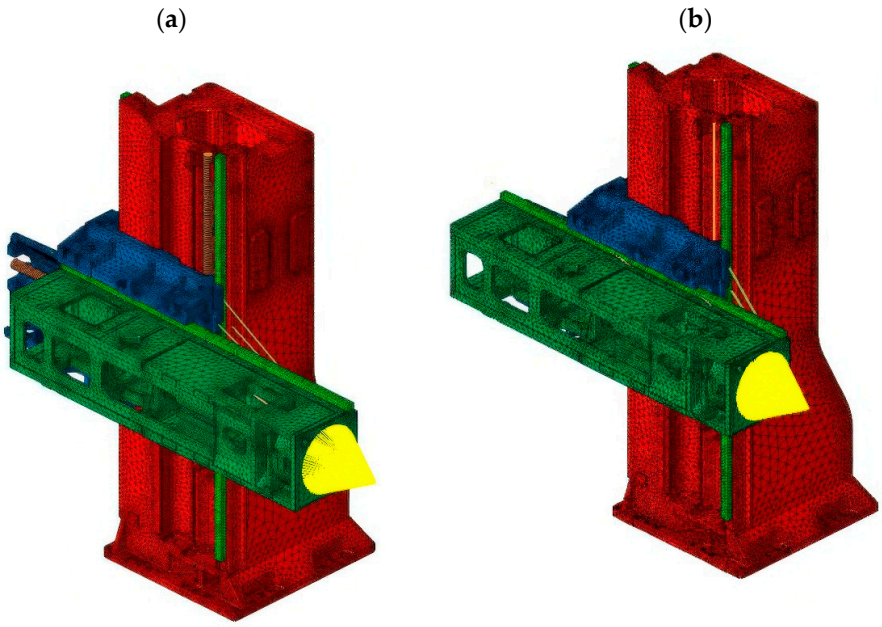

Figure 21. ZERO™ FEM calculated positions: (**a**) Position 1—maximum Y travel, and (**b**) Position 2—Intermediate Y travel.

Figure 22 illustrates the measured data and the FEM model output obtained using the ambient temperature variations recorded during the test conducted from 23 to 26 February. The graph represents the measured E_Y error evolution at Point P_11 alongside the FEM-

simulated value. This specific point corresponds to the maximum extension of the ram (Point 11 in Figure 14 and Position 1 in Figure 21a).

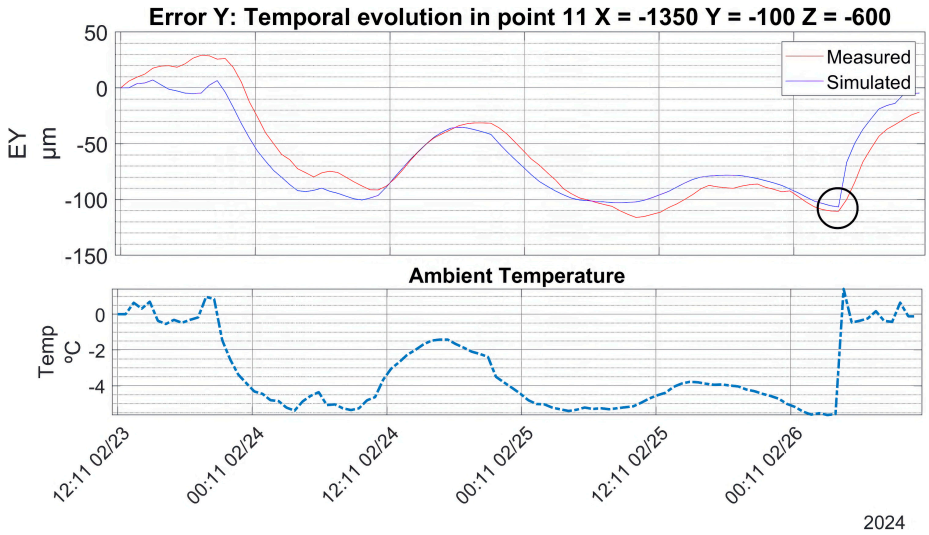

Figure 22. FEM simulation vs measured data: second test, from 23 to 26 February. Position 1 (maximum ram extension).

Figure 23 presents the FEM results in the Y direction in the specific moment indicated with a circle in Figure 22, which is near the conclusion of the test, when the machine responds to the activation of the heating system and the error begins to reduce. The undeformed and deformed structures are displayed together in the image, illustrating how the contraction of the ram predominantly contributes to the error in the Y direction. The corresponding error values are also plotted.

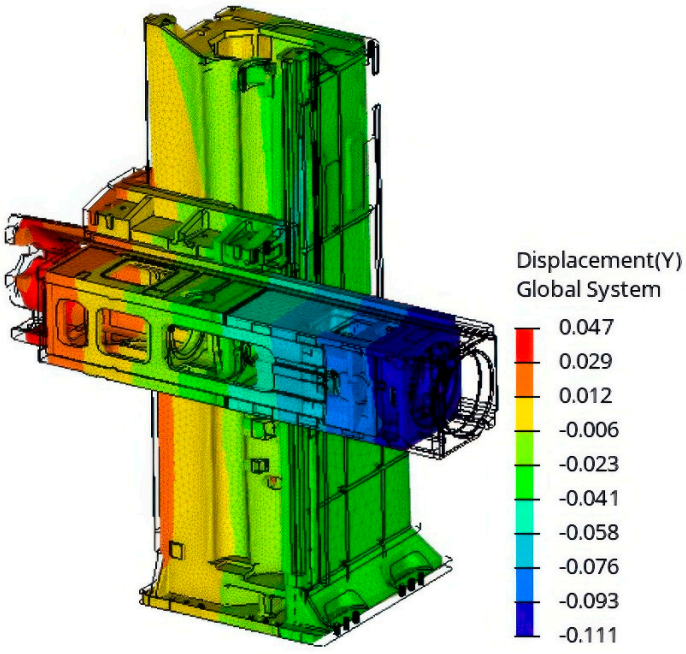

Figure 23. FEM-simulated Y error (mm). Second test, from 23 to 26 February. Position 1 (maximum ram extension).

Figure 24 illustrates the measured data and the FEM model output obtained using the ambient temperature variations recorded during the test conducted from 23 to 26 February. The graph represents the measured E_Y error evolution at point 31 alongside the FEM-

simulated value. This specific point corresponds to the intermediate extension of the ram (Point 31 in Figure 14, Position 2 in Figure 21b).

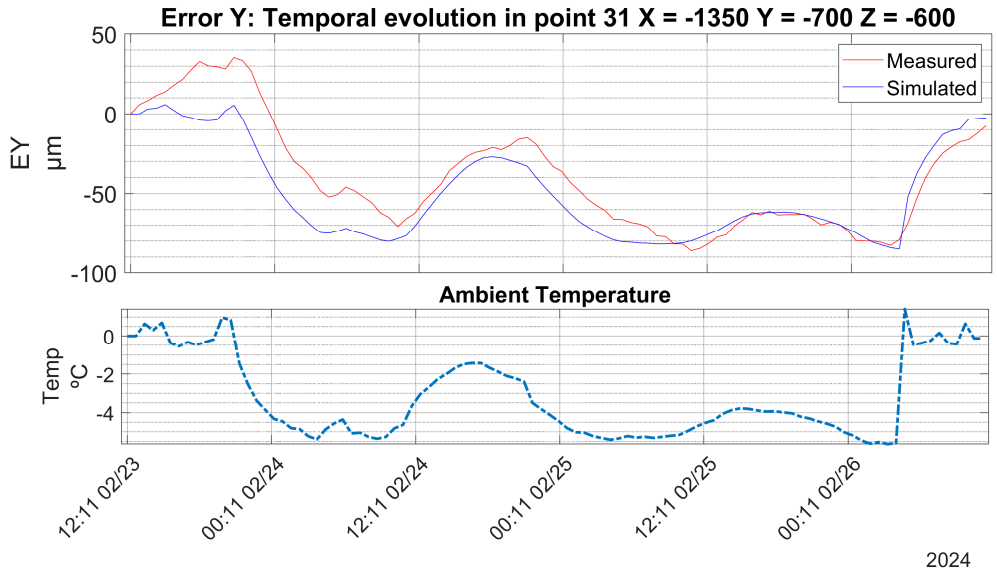

Figure 24. FEM simulation vs measured data. Second test, from 23 to 26 February. Position 2 (intermediate ram extension).

The FEM-based validation of the ZERO™ machine tests has demonstrated a strong correlation between the simulated and measured thermal error evolutions, with the FEM model accurately capturing the influence of environmental temperature variations on the Y-axis position errors. The comparison of the measured data with the FEM simulation results, particularly at critical positions such as the maximum and intermediate Y-axis travel, shows a good agreement, confirming the reliability of the simulation in predicting machine behaviour under varying environmental conditions.

Table 10 presents the numerical values of the established metrics for comparing the measured data with the values calculated by the FEM model for the two defined positions. At Position 1 (maximum Y travel), the FEM model effectively reproduced the significant thermal error changes induced by the temperature fluctuations, with both the mean absolute error (MAE) and root mean square error (RMSE) values indicating a satisfactory level of accuracy (13.1 µm and 16.3 µm, respectively). Similar correlations were observed at Position 2 (intermediate Y travel), with the MAE and RMSE values of 13.3 µm and 17.3 µm, respectively, further validating the robustness of the FEM model.

Table 10. Comparison metrics between measured values and FEM model predictions.

	Travel Y (mm)	MAE [µm]	RMSE [µm]
Position 1	−1350	13.1	16.3
Position 2	−700	13.3	17.3

4. Conclusions

This study extends previous research by further developing the machine tool integrated inverse multilateration (MIIM) methodology to assess the impact of ambient thermal variations on medium- and large-scale machine tools in industrial environments. By embedding an absolute distance measurement device within the spindle, the MIIM methodology provides an automated approach to volumetric error characterisation, eliminating reliance on controlled conditions, expensive thermal monitoring equipment, or dedicated calibra-

tion artefacts. This advancement makes the MIIM method a practical tool for evaluating thermal distortions in real-world manufacturing settings.

The methodology has been applied to the assessment of large-scale machine tools operating under fluctuating thermal conditions, offering a reliable and scalable solution for automated error evaluation. Its adaptability to different machine configurations, control systems, and environmental conditions underscores its potential for broad industrial application.

Comprehensive testing has demonstrated the robustness of the MIIM method, facilitating continuous, unattended data collection over extended periods. The results confirm its effectiveness in detecting thermally induced errors in large machine tools while addressing critical challenges in thermal error assessment, such as the need for low measurement uncertainty, full volumetric coverage, and the efficient monitoring of temperature-related deviations.

Validation experiments were conducted on two distinct machine architectures—THERA™ (gantry type) and ZERO™ (bed type)—within standard workshop conditions, without altering the ambient environment. These trials complement earlier investigations involving the ARION G™ (bridge type) machine, reinforcing the MIIM method's applicability across diverse machining platforms. Long-term testing revealed a strong correlation between thermal error patterns and ambient temperature fluctuations, validating the methodology's reliability for autonomous monitoring over extended durations.

Further validation was achieved through a combination of first-order analytical models and finite element simulations, confirming ambient temperature variations as the primary driver of the observed thermal deviations. This integration of experimental data with simulation models strengthens the foundation for future refinements in machine tool performance optimisation and thermal compensation strategies.

The principal outcomes of this research include:

- Applicability to large MTs: The investigations using gantry- and bed-type machines, alongside prior work on bridge-type machines, demonstrate the methodology's applicability to large-scale MTs;
- Customisable parameters: Measurement points and traversal paths can be tailored to the experimental objectives, enabling rapid measurements during fast temperature changes or a higher resolution during gradual variations;
- Full automation: The system operates autonomously, enabling continuous measurement cycles without manual intervention and allowing hundreds of measurements to be conducted consecutively over multiple days;
- Controller compatibility: The system supports HEIDENHAIN and SIEMENS controllers, demonstrating versatility across different machine setups;
- Thermal dynamics insights: The MIIM method identifies critical parameters such as the frequency, amplitude, and temperature gradients of ambient air temperature changes, aligning with the ISO 230-3:2020 standards [29] and enhancing its industrial relevance.

The ability of the MIIM method to characterise volumetric errors within a 40 to 60 min cycle significantly enhances its practicality for various industrial applications. It is particularly suited for rapid quality control during factory acceptance testing, the comprehensive evaluation of new machine designs, and the precision assessment of machine installations in non-thermally regulated environments.

Collaboration with Zayer MT builder has reinforced the industry relevance of MIIM, highlighting its practical benefits for machine tool manufacturers. To facilitate widespread adoption, future efforts should focus on developing a cost-effective CNC-based distance-

measurement instrument with enhanced accuracy, which would further strengthen the applicability of the MIIM method in industrial settings.

Author Contributions: Conceptualization, investigation, and writing—original draft, F.E.; supervision and writing—review and editing, J.A.Y.-F.; conceptualization and writing—review and editing U.M.; formal analysis B.A.C.; formal analysis S.L. All authors have read and agreed to the published version of the manuscript.

Funding: This research received no external funds.

Institutional Review Board Statement: Not applicable.

Informed Consent Statement: Not applicable.

Data Availability Statement: The data presented in this study are available on request from the corresponding author due to restrictions imposed by Zayer to perform this research using their machine.

Acknowledgments: The authors express their gratitude for the invaluable support provided by Zayer and the special agreement established with TEKNIKER, enabling the research conducted using their THERA^{TM} and ZERO^{TM} machines.

Conflicts of Interest: The authors declare no conflicts of interest.

References

1. Bryan, J. International Status of Thermal Error Research. *CIRP Ann. Manuf. Technol.* **1969**, *16*, 203–215.
2. Mayr, J.; Jedrzejewski, J.; Uhlmann, E.; Alkan Donmez, M.; Knapp, W.; Härtig, F.; Wendt, K.; Moriwaki, T.; Shore, P.; Schmitt, R.; et al. Thermal Issues in Machine Tools. *CIRP Ann. Manuf. Technol.* **2012**, *61*, 771791. [CrossRef]
3. Gao, W.; Ibaraki, S.; Donmez, M.A.; Kono, D.; Mayer, J.R.R.; Chen, Y.L.; Szipka, K.; Archenti, A.; Linares, J.M.; Suzuki, N. Machine Tool Calibration: Measurement, Modeling, and Compensation of Machine Tool Errors. *Int. J. Mach. Tools Manuf.* **2023**, *187*, 104017. [CrossRef]
4. Ramesh, R.; Mannan, M.A.; Poo, A.N. Error Compensation in Machine Tools—A Review Part II: Thermal Errors. *Int. J. Mach. Tools Manuf.* **2000**, *40*, 1257–1284. [CrossRef]
5. Schwenke, H.; Knapp, W.; Haitjema, H.; Weckenmann, A.; Schmitt, R.; Delbressine, F. Geometric Error Measurement and Compensation of Machines—An Update. *CIRP Ann. Manuf. Technol.* **2008**, *57*, 660–675. [CrossRef]
6. Ibaraki, S.; Knapp, W. Indirect Measurement of Volumetric Accuracy for Three-Axis and Five-Axis Machine Tools A Review Indirect Measurement of Volumetric Accuracy for Three-Axis and Five-Axis Machine Tools: A Review. *Int. J. Autom. Technol.* **2012**, *6*, 110–124. [CrossRef]
7. Li, Y.; Yu, M.; Bai, Y.; Hou, Z.; Wu, W. A Review of Thermal Error Modeling Methods for Machine Tools. *Appl. Sci.* **2021**, *11*, 5216. [CrossRef]
8. Wang, Y.; Cao, Y.; Qu, X.; Wang, M.; Wang, Y.; Zhang, C. A Review of the Application of Machine Learning Techniques in Thermal Error Compensation for CNC Machine Tools. *Measurement* **2025**, *243*, 116341. [CrossRef]
9. Uriarte, L.; Zatarain, M.; Axinte, D.; Yague-Fabra, J.; Ihlenfeldt, S.; Eguia, J.; Olarra, A. Machine Tools for Large Parts. *CIRP Ann. Manuf. Technol.* **2013**, *62*, 731–750. [CrossRef]
10. Schmitt, R.; Peterek, M. Traceable Measurements on Machine Tools-Thermal Influences on Machine Tool Structure and Measurement Uncertainty. *Procedia CIRP* **2015**, *33*, 576–580. [CrossRef]
11. Mian, N.S.; Fletcher, S.; Longstaff, A.P.; Myers, A. Efficient Estimation by FEA of Machine Tool Distortion Due to Environmental Temperature Perturbations. *Precis. Eng.* **2013**, *37*, 372–379. [CrossRef]
12. Brecher, C.; Behrens, J.; Klatte, M.; Lee, T.H.; Tzanetos, F. Measurement and Analysis of Thermo-Elastic Deviation of Five-Axis Machine Tool Using Dynamic R-Test. *Procedia CIRP* **2018**, *77*, 521–524. [CrossRef]
13. Gross, L.; Held, C.; Keller, F.; Wendt, K.; Franke, M.; Gerwien, N. Mapping and Compensation of Geometric Errors of a Machine Tool at Different Constant Ambient Temperatures. *Precis. Eng.* **2020**, *63*, 10–17. [CrossRef]
14. Wei, X.; Ye, H.; Feng, X. Year-Round Thermal Error Modeling and Compensation for the Spindle of Machine Tools Based on Ambient Temperature Intervals. *Sensors* **2022**, *22*, 5085. [CrossRef] [PubMed]
15. Wei, X.; Ye, H.; Zhou, J.; Pan, S.; Qian, M. A Regularized Regression Thermal Error Modeling Method for CNC Machine Tools under Different Ambient Temperatures and Spindle Speeds. *Sensors* **2023**, *23*, 4916. [CrossRef] [PubMed]

16. Breitzke, A.; Hintze, W. Workshop-Suited Identification of Thermo-Elastic Errors of Three-Axis Machine Tools Using on-Machine Measurement. *Precis. Eng.* **2024**, *85*, 72–88. [CrossRef]
17. Wei Kert', S. R-Test, a New Device for Accuracy Measurements on Five Axis Machine Tools. *CIRP Ann.* **2004**, *53*, 429–432. [CrossRef]
18. Iñigo, B.; Ibabe, A.; de Lacalle, L.N.L.; Aguirre, G. Characterization and Uncertainty Analysis of Volumetric Error Variation with Temperature. *Precis. Eng.* **2023**, *81*, 167–182. [CrossRef]
19. Iñigo, B.; Colinas-Armijo, N.; López de Lacalle, L.N.; Aguirre, G. Digital Twin for Volumetric Thermal Error Compensation of Large Machine Tools. *Sensors* **2024**, *24*, 6196. [CrossRef]
20. Schwenke, H.; Franke, M.; Hannaford, J.; Kunzmann, H. Error Mapping of CMMs and Machine Tools by a Single Tracking Interferometer. *CIRP Ann. Manuf. Technol.* **2005**, *54*, 475–478. [CrossRef]
21. Ibaraki, S.; Blaser, P.; Shimoike, M.; Takayama, N.; Nakaminami, M.; Ido, Y. Measurement of Thermal Influence on a Two-Dimensional Motion Trajectory Using a Tracking Interferometer. *CIRP Ann. Manuf. Technol.* **2016**, *65*, 483–486. [CrossRef]
22. Mori, M.; Irino, N.; Shimoike, M. A New Measurement Method for Machine Tool Thermal Deformation on a Two-Dimensional Trajectory Using a Tracking Interferometer. *CIRP Ann.* **2019**, *68*, 551–554. [CrossRef]
23. Maruyama, D.; Ibaraki, S. A Single-Axis Tracking Interferometer to Measure Two-Dimensional Error Motions of Machine Tools and Industrial Robots. *Measurements* **2025**, *245*, 116548. [CrossRef]
24. Guillory, J.; Truong, D.; Wallerand, J.P.; Alexandre, C. Absolute Multilateration-Based Coordinate Measurement System Using Retroreflecting Glass Spheres. *Precis. Eng.* **2022**, *73*, 214–227. [CrossRef]
25. Javier Brosed, F.; José Aguilar, J.; Acero, R.; Santolaria, J.; Aguado, S.; Pueo, M. Calibration and Uncertainty Budget Analysis of a High Precision Telescopic Instrument for Simultaneous Laser Multilateration. *Measurement* **2022**, *190*, 110735. [CrossRef]
26. Schwenke, H. Large Parts with Critical Tolerances: Concepts and Possible Solutions for Traceable CMM Measurements on Machine Tools. In Proceedings of the Traceable In-Process Dimensional Measurement Final Workshop, Braunschweig, Germany, 18 May 2016.
27. Schmitt, R.; Peterek, M.; Quinders, S. Concept of a Virtual Metrology Frame Based on Absolute Interferometry for Multi Robotic Assembly. In *Precision Assembly Technologies and Systems*; Ratchev, S., Ed.; IFIP Advances in Information and Communication Technology Series 435; Springer: Berlin/Heidelberg, Germany, 2014; pp. 79–86.
28. Brecher, C.; Spierling, R.; Fey, M.; Neus, S. Direct Measurement of Thermo-Elastic Errors of a Machine Tool. *CIRP Ann.* **2021**, *70*, 333–336. [CrossRef]
29. *ISO 230-3:2020*; Test Code for Machine Tools—Part 3: Determination of Thermal Effects. International Organization for Standardization: Geneva, Switzerland, 2020.
30. Egaña, F.; Yagüe-Fabra, J.A.; Mutilba, U.; Vez, S. Machine Tool Integrated Inverse Multilateration Uncertainty Assessment for the Volumetric Characterisation and the Environmental Thermal Error Study of Large Machine Tools. *CIRP Ann.* **2021**, *70*, 435–438. [CrossRef]
31. Egaña, F.; Yagüe-Fabra, J.A.; Mutilba, U.; Eguskiza, J. The MIIM Method for the Environmental Thermal Error Study of Large Machine Tools: A Real Case Study. In Proceedings of the EUSPEN'S 22nd International Conference & Exhibition, Geneva, Switzerland, 30 May–3 June 2022; pp. 145–148.
32. Egaña, F.; Mutilba, U.; Kortaberria, G.; Eguskiza, J.; Check, B.A. From the Traditional Multilateration To the Integrated Multilateration Approach: A Roadmap Towards the Automatization of Volumetric Error Mapping Process for Large Machine Tools. *MM Sci. J.* **2023**, *2023*, 6909–6914. [CrossRef]
33. Egaña, F.; Mutilba, U.; Yagüe-Fabra, J.A.; Gomez-acedo, E. A Novel Methodology for Measuring Ambient Thermal Effects on Machine Tools. *Sensors* **2024**, *24*, 2380. [CrossRef]
34. Mutilba, U.; Yagüe-Fabra, J.A.; Gomez-Acedo, E.; Kortaberria, G.; Olarra, A. Integrated Multilateration for Machine Tool Automatic Verification. *CIRP Ann.* **2018**, *67*, 555–558. [CrossRef]
35. Zhang, C.; Gao, F.; Yan, L. Thermal Error Characteristic Analysis and Modeling for Machine Tools Due to Time-Varying Environmental Temperature. *Precis. Eng.* **2017**, *47*, 231–238. [CrossRef]
36. Mian, N.S.; Fletcher, S.; Longstaff, A.P.; Myers, A. Efficient Thermal Error Prediction in a Machine Tool Using Finite Element Analysis. *Meas. Sci. Technol.* **2011**, *22*, 085107. [CrossRef]
37. Leica. *Leica Absolute Tracker AT930 Brochure*; Leica Geosystems AG: Heerbrugg, Switzerland, 2021.
38. *DIN EN 1561:2024-03*; Founding—Grey Cast Irons. German Version; Beuth Verlag GmbH: Berlin, Germany, 2024.